Title	Nonlinear wave growth theory of coherent hiss emissions in the plasmasphere
Author(s)	Omura, Yoshiharu; Nakamura, Satoko; Kletzing, Craig A.; Summers, Danny; Hikishima, Mitsuru
Citation	Journal of Geophysical Research: Space Physics (2015), 120(9): 7642-7657
Issue Date	2015-09
URL	http://hdl.handle.net/2433/203040
Right	Accepted for publication in 'Journal of Geophysical Research: Space Physics'. Copyright (year) American Geophysical Union. Further reproduction or electronic distribution is not permitted.; The full-text file will be made open to the public on 29 March 2016 in accordance with publisher's 'Terms and Conditions for Self-Archiving'.
Type	Journal Article
Textversion	publisher

Nonlinear wave growth theory of coherent hiss emissions in the plasmasphere

Yoshiharu Omura[1], Satoko Nakamura[2], Craig A. Kletzing[3], Danny Summers[1,4], and Mitsuru Hikishima[5,6]

[1]Research Institute for Sustainable Humanosphere, Kyoto University, Kyoto, Japan, [2]Department of Geophysics, Graduate School of Science, Kyoto University, Kyoto, Japan, [3]Department of Physics and Astronomy, University of Iowa, Iowa City, Iowa, USA, [4]Department of Mathematics and Statistics, Memorial University of Newfoundland, St. John's, Newfoundland, Canada, [5]Solar-Terrestrial Environment Laboratory, Nagoya University, Nagoya, Japan, [6]Institute of Space and Astronautical Science, Japan Aerospace Exploration Agency, Sagamihara, Japan

Abstract Recent observations of plasmaspheric hiss emissions by the Van Allen Probes show that broadband hiss emissions in the plasmasphere comprise short-time coherent elements with rising and falling tone frequencies. Based on nonlinear wave growth theory of whistler mode chorus emissions, we have examined the applicability of the nonlinear theory to the coherent hiss emissions. We have generalized the derivation of the optimum wave amplitude for triggering rising tone chorus emissions to the cases of both rising and falling tone hiss elements. The amplitude profiles of the hiss emissions are well approximated by the optimum wave amplitudes for triggering rising or falling tones. Through the formation of electron holes for rising tones and electron hills for falling tones, the coherent waves evolve to attain the optimum amplitudes. An electromagnetic particle simulation confirms the nonlinear wave growth mechanism as the initial phase of the hiss generation process. We find very good agreement between the theoretical optimum amplitudes and the observed amplitudes as a function of instantaneous frequency. We calculate nonlinear growth rates at the equator and find that nonlinear growth rates for rising tone emissions are much larger than the linear growth rates. The time scales of observed hiss emissions also agree with those predicted by the nonlinear theory. Based on the theory, we can infer properties of energetic electrons generating hiss emissions in the equatorial region of the plasmasphere.

1. Introduction

Plasmaspheric hiss emissions, which are low-frequency electromagnetic whistler mode waves with broadband spectra, have been observed by many spacecraft, and there have been many studies on possible generation mechanisms of the hiss emissions. Most of these generation mechanisms assume wave growth due to linear growth rates of Doppler-shifted cyclotron resonance [*Kennel and Petschek*, 1966] driven by temperature anisotropy of energetic electrons in the plasmasphere [*Thorne et al.*, 1973]. The seeds of the instability derive from thermal fluctuations [*Chen et al.*, 2014] or an external source coming from outside of the plasmasphere such as either whistlers induced by lightning [*Dragonov et al.*, 1992] or whistler mode chorus emissions generated in a source region located close to the geomagnetic equator outside the plasmasphere [*Santolik et al.*, 2006]. The external sources have been assumed because of the very low gain attained by path integration of convective wave growth based on the linear growth rate [*Huang et al.*, 1983; *Church and Thorne*, 1983]. Based on spacecraft observations and ray tracing study, on the other hand, *Bortnik et al.* [2008, 2009] proposed that hiss waves are chorus waves that have propagated into the plasmapause.

Recent observations by the Electric and Magnetic Field Instrument Suite and Integrated Science (EMFISIS) instrument on the Van Allen Probes [*Kletzing et al.*, 2013] show unusual enhancement of the low-frequency part of plasmaspheric hiss in the outer plasmasphere associated with substorm-injected electrons [*Li et al.*, 2013; *Ni et al.*, 2014]. *Summers et al.* [2014] have reported fine structures embedded in the spectrograms of hiss emissions observed by EMFISIS. These hiss emissions have a common feature that the lowest-frequency part has the highest intensity with a profile of decreasing amplitude with increasing frequency, as shown in Figure 1f of *Ni et al.* [2014] and Figure 13 of *Summers et al.* [2014]. This feature was also found in the early observations by OGO 5 and was described as a sharp low-frequency cutoff [*Thorne et al.*, 1973].

Inspired by the fine structures of hiss emissions reported by *Summers et al.* [2014], which resemble small segments of rising tone and falling tone chorus emissions, we have checked the theoretical amplitude profile for chorus emissions [*Omura and Nunn*, 2011] for a large ratio of the electron plasma frequency to the electron cyclotron frequency. We find a remarkable similarity between the profile of hiss amplitudes and the optimum amplitude for triggering rising tone emissions. We present a possible interpretation of the plasmaspheric hiss emissions based on nonlinear wave growth theory. We first derive optimum and threshold amplitudes for nonlinear growth of discrete hiss emissions in section 2. We study the initial phase of the generation process of hiss emissions by performing a particle simulation in section 3. In section 4 hiss wave data from the Van Allen Probes are presented together with theoretical estimates of the wave amplitudes, frequency sweep rates, and nonlinear transition time for triggering rising tone and falling tone hiss elements. In section 5 we present a summary and discussion.

2. Nonlinear Wave Growth Theory of Hiss Emissions

Observations by Polar [*Santolik et al.*, 2001], Cluster [*Laakso et al.*, 2015], and the Van Allen Probes [*Summers et al.*, 2014] indicate that wave normal vectors of the plasmaspheric hiss emissions are nearly parallel to the background magnetic field near the magnetic equator. We assume a number of coherent whistler mode waves propagating parallel to the background magnetic field with different frequencies ω^j ($j = 1, 2, 3, \ldots, n$) ordered from low to higher frequencies at the same position and time. These waves correspond to different cyclotron resonance velocities V_R^j. A trapping potential is formed around each resonance velocity V_R^j with a width of the trapping velocity V_{tr}^j [*Omura et al.*, 1991]. Electrons with parallel velocities $v_\parallel$ that satisfy

$$V_R^j - V_{tr}^j < v_\parallel < V_R^j + V_{tr}^j \tag{1}$$

interact with the wave with frequency ω^j effectively, and their motions are strongly modified, resulting in the depletion or enhancement of its resonant electrons in velocity phase space. The depletion is called an electron hole generating a rising tone emission [*Omura et al.*, 2008, 2012], while the enhancement is called an electron hill generating a falling tone [*Nunn and Omura*, 2012; *Omura et al.*, 2012]. Provided that any adjacent pair of resonance velocities V_R^j and V_R^{j+1} ($j = 1, 2, 3, \ldots, n - 1$) are separated with a spacing much greater than a sum of the corresponding trapping velocities $V_{tr}^j + V_{tr}^{j+1}$, i.e.,

$$|V_R^{j+1} - V_R^j| \gg V_{tr}^j + V_{tr}^{j+1}, \tag{2}$$

the motion of energetic electrons with parallel velocities close to the resonance velocity V_R^j can be described as an interaction with a single coherent wave with frequency ω^j. In the following, we will make use of this approximation, assuming that the separability criterion (2) is satisfied. For simplicity, we neglect the superscript j corresponding to each of the waves.

2.1. Optimum Amplitude for Generating Discrete Hiss Emissions

We assume a coherent whistler mode wave propagating parallel to the background magnetic field $\boldsymbol{B_0}$ with a wave number k and a frequency ω_0 satisfying the linear dispersion relation

$$c^2 k^2 - \omega_0^2 - \frac{\omega_0 \omega_{pe}^2}{\Omega_e - \omega_0} = 0, \tag{3}$$

where c, Ω_e, and ω_{pe} are the speed of light, the electron cyclotron frequency, and the electron plasma frequency, respectively. We introduce the dimensionless parameters χ and ξ defined by

$$\chi^2 = 1 - \frac{\omega_0^2}{c^2 k^2}, \tag{4}$$

and

$$\xi^2 = \frac{\omega_0(\Omega_e - \omega_0)}{\omega_{pe}^2}. \tag{5}$$

The cold plasma dispersion relation (3) is rewritten as

$$\chi^2 = \frac{1}{1 + \xi^2}. \tag{6}$$

The phase velocity $V_p = \omega_0/k$, the resonance velocity V_R, and the group velocity $V_g = \partial\omega_0/\partial k$ are given by the respective equations [*Omura et al.*, 2008, 2012],

$$\tilde{V}_p = V_p/c = \chi\xi, \tag{7}$$

$$\tilde{V}_R = V_R/c = -\chi\xi\left(\frac{\Omega_e}{\gamma\omega_0} - 1\right), \tag{8}$$

and

$$\tilde{V}_g = V_g/c = \frac{\xi}{\chi}\left[\xi^2 + \frac{\Omega_e}{2(\Omega_e - \omega_0)}\right]^{-1}, \tag{9}$$

where we assume $V_p > 0$ with $k > 0$. In these equations the wave number k, which is difficult to measure by observation, has been eliminated by using the cold plasma dispersion relation.

We assume that the velocity distribution function f of hot energetic electrons is given in terms of the relativistic momentum per unit mass $u = \gamma v$; u has components $u_\parallel = \gamma v_\parallel$ and $u_\perp = \gamma v_\perp$, respectively, parallel and perpendicular to the background magnetic field. For simplicity in developing nonlinear theory, we assume f to take the form

$$f(u_\parallel, u_\perp) = \frac{N_h}{(2\pi)^{3/2}U_{t\parallel}U_{\perp 0}}\exp\left(-\frac{u_\parallel^2}{2U_{t\parallel}^2}\right)\Delta(u_\perp - U_{\perp 0}), \tag{10}$$

where $U_{\perp 0} = \gamma V_{\perp 0}$, $U_{t\parallel}$ is the thermal momentum in the parallel direction, Δ is the Dirac delta function, and we have normalized f to the density of hot electrons N_h.

We assume that energetic electrons less than a few hundred keV interact with a coherent whistler mode wave with frequency ω near the magnetic equator and that they satisfy the condition $\gamma < \Omega_e/\omega$. From (8), we find $V_R < 0$, and the resonant electrons move opposite to the direction of the wave packets. The resonant electrons interacting with the wave packet fall into two groups, trapped and untrapped resonant electrons. Trapped resonant electrons are guided along the resonance velocity V_R. For a rising tone wave packet, $|V_R|$ becomes small and the counterstreaming trapped electrons are guided to the higher density part of the reduced velocity distribution function $F(v_\parallel)$, thereby resulting in a depletion around V_R, i.e., an electron hole is created, as illustrated in red in Figure 1a. For a falling tone wave packet, on the other hand, $|V_R|$ becomes larger and the trapped electrons are guided to the lower density part of the distribution function, resulting in an enhanced density around V_R, i.e., an electron hill is formed as illustrated in blue in Figure 1a.

Integrating $f(u_\parallel, u_\perp)$ over $u_\perp$ and taking an average over ζ, we obtain the unperturbed distribution function $g_0(v_\parallel)$ as

$$g_0(v_\parallel) = \frac{N_h}{(2\pi)^{3/2}U_{t\parallel}U_{\perp 0}}\exp\left(-\frac{\gamma^2 v_\parallel^2}{2U_{t\parallel}^2}\right). \tag{11}$$

We assume a distribution of the trapped resonant electrons $g_t(v_\parallel, \zeta)$. Depletion of the trapped electrons results in the distribution function,

$$g(v_\parallel, \zeta) = g_0(v_\parallel) - Qg_t(v_\parallel, \zeta), \tag{12}$$

where Q represents the depth of the electron hole [*Omura et al.*, 2009, 2012]. We can express an enhancement of the phase-trapped electrons by a negative value of Q [*Nunn and Omura*, 2012]. The electron hole and electron hill in velocity phase space $(v_\parallel, \zeta)$ are illustrated in Figure 1b, where ζ is an angle between the perpendicular velocity of a resonant electron and the wave magnetic field. The dynamics of a resonant electron are described by the equations,

$$\frac{d\zeta}{dt} = k(v_\parallel - V_R), \tag{13}$$

and

$$k\frac{d(v_\parallel - V_R)}{dt} = \omega_{tr}^2(\sin\zeta + S), \tag{14}$$
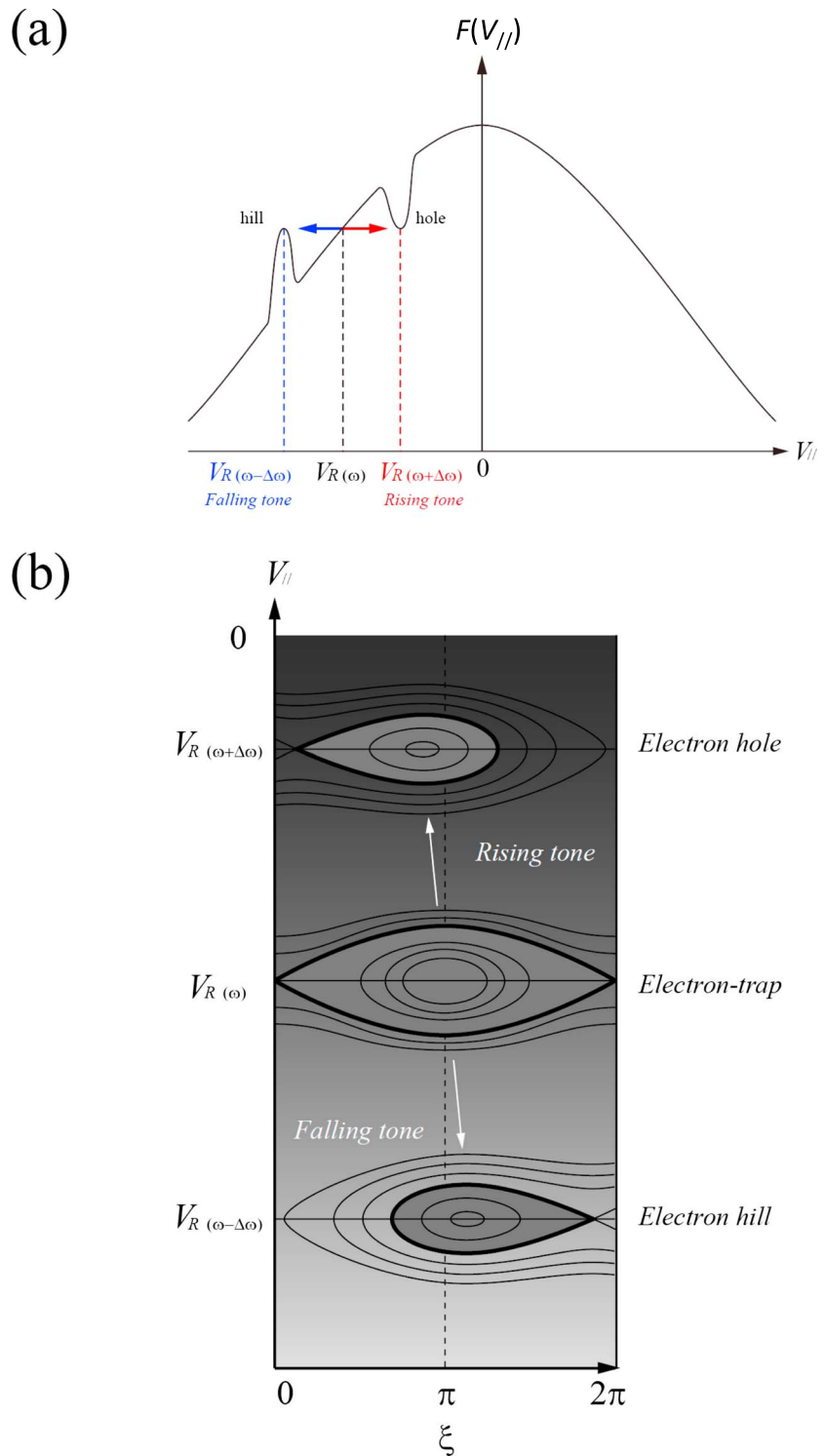
Figure 1. (a) Formation of an electron hole due to a rising tone element and an electron hill due to a falling tone element in the reduced velocity distribution function $F(v_{\|})$ of energetic electrons at the equator and (b) the corresponding variations of $g(v_{\|}, \zeta)$ in velocity phase space $(v_{\|}, \zeta)$.

where $\omega_{tr} = \chi \sqrt{kV_{\perp 0}\Omega_w/\gamma}$, and the parameter S is an inhomogeneity factor given by

$$S = -\frac{1}{s_0\omega_0\Omega_w}\left(s_1\frac{\partial\omega}{\partial t} + cs_2\frac{\partial\Omega_e}{\partial h}\right),$$ (15)

where

$$s_0 = \frac{\chi}{\xi}\tilde{V}_{\perp 0},$$ (16)

$$s_1 = \gamma\left(1 - \frac{\tilde{V}_R}{\tilde{V}_g}\right)^2,$$ (17)

and

$$s_2 = \frac{1}{2\xi\chi}\left\{\frac{\gamma\omega_0}{\Omega_e}\tilde{V}_{\perp 0}^2 - \left[2 + \frac{\chi^2(\Omega_e - \gamma\omega_0)}{\Omega_e - \omega_0}\right]\tilde{V}_R\tilde{V}_p\right\}.$$ (18)

In calculating s_2, we assume that the cold plasma density is constant along the magnetic field line.

With a constant wave frequency, the trapping potential is symmetric around $\zeta = \pi$, while the potential is deformed with a rising or falling frequency, as shown in Figure 1b.

We calculate the resonance currents J_E and J_B parallel to the wave electric and magnetic field components, respectively, as

$$J_E = -eQV_{\perp 0}^2\int_0^{2\pi}\int_{-\infty}^{\infty}g_t(v_\parallel, \zeta)\sin\zeta\, dv_\parallel d\zeta,$$ (19)

$$J_B = eQV_{\perp 0}^2\int_0^{2\pi}\int_{-\infty}^{\infty}g_t(v_\parallel, \zeta)\cos\zeta\, dv_\parallel d\zeta.$$ (20)

Assuming a nonlinear trapping potential of a wave with a varying frequency, we express the resonant currents as

$$J_E = -J_0\int_{\zeta_1}^{\zeta_2}[\cos\zeta_1 - \cos\zeta + S(\zeta - \zeta_1)]^{1/2}\sin\zeta\, d\zeta,$$ (21)

and

$$J_B = J_0\int_{\zeta_1}^{\zeta_2}[\cos\zeta_1 - \cos\zeta + S(\zeta - \zeta_1)]^{1/2}\cos\zeta\, d\zeta,$$ (22)

where $J_0 = (2e)^{3/2}(m_0k\gamma)^{-1/2}V_{\perp 0}^{5/2}\chi QGB_w^{1/2}$, and e and m_0 are the charge and rest mass of an electron. The phase angles ζ_1 and ζ_2 define the boundary of the trapping wave potential, as described by *Omura et al.* [2009, 2012]. The parameter G is the value of the velocity distribution function $g(v_\parallel, \zeta)$ in the trapping region around the resonance velocity.

Omura et al. [2008] found that the maximum value of $-J_E$ takes place when $S = -0.4$ for a rising tone, and *Nunn and Omura* [2012] also found that the maximum value of $-J_E$ takes place when $S = 0.4$ for a falling tone. In either case, we find $J_B = -1.3J_0$, which can be written as

$$J_B = -1.3(2e)^{3/2}\left(\frac{B_w}{m_0k\gamma}\right)^{1/2}V_{\perp 0}^{5/2}\chi QG.$$ (23)

We note that the sign of J_B is determined by the sign of Q. From the relation connecting the nonlinear frequency deviation ω_1 and J_B,

$$\omega_1 = -\frac{\mu_0 V_g}{2}\frac{J_B}{B_w},$$ (24)

we find that a positive or negative Q corresponds to a rising or falling tone, respectively.

The nonlinear transition time T_N for the formation of the nonlinear resonant current is roughly estimated by the nonlinear trapping period T_{tr} given by

$$T_{tr} = \frac{2\pi}{\omega_{tr}} = \frac{2\pi}{\chi}\left(\frac{m_0\gamma}{kV_{\perp 0}eB_w}\right)^{1/2},$$ (25)

where ω_{tr} is the trapping frequency [*Omura et al.*, 2008, 2012]. We define the ratio $\tau = T_N/T_{tr}$, which we will determine by comparison with plasmaspheric hiss observations below.

Over the nonlinear transition time T_N, the electron hole or hill is gradually formed. Along with the formation of J_B, the frequency of the triggered wave gradually deviates from ω_0 to $\omega_0 + \omega_1$. From (11), (23), and (25), we obtain the averaged frequency sweep rate over the nonlinear trapping period as

$$\frac{\omega_1}{T_N} = \frac{1.3}{4}\pi^{-5/2}\frac{Q}{\tau}\left(\frac{\chi\omega_{ph}V_{\perp 0}}{\gamma c}\right)^2\frac{V_g}{U_{t\parallel}}\exp\left(-\frac{\gamma^2 V_R^2}{2U_{t\parallel}^2}\right),$$ (26)

where ω_{ph} is the plasma frequency of the hot energetic electrons defined by $\omega_{ph}^2 = \mu_0 c^2 N_h e^2/m_0$.

At the equator the inhomogeneity of the magnetic field is zero, and the second term on the right-hand side of (15) vanishes. From (15) we can derive the relation between the frequency sweep rate and the normalized wave amplitude $\Omega_w = eB_w/m_0$ at the equator in the form,

$$\frac{\partial\omega}{\partial t} = -\frac{Ss_0\omega_0}{s_1}\Omega_w.$$ (27)

Equating the left-hand sides of (26) and (27), and with $|S| = 0.4$ for the maximum value of $|J_E|$, we obtain the optimum wave amplitude Ω_{wo} that can trigger a rising tone ($\omega_1 > 0$) or falling tone ($\omega_1 < 0$) hiss element as

$$\Omega_{wo} = \frac{s_1|\omega_1|}{0.4s_0\omega_0 T_N}.$$ (28)

From (26) and (28), we obtain

$$\tilde{\Omega}_{wo} = 0.81\pi^{-5/2}\frac{|Q|}{\tau}\frac{s_1\tilde{V}_g}{s_0\tilde{\omega}_0\tilde{U}_{t\parallel}}\left(\frac{\chi\tilde{\omega}_{ph}\tilde{V}_{\perp 0}}{\gamma}\right)^2\exp\left(-\frac{\gamma^2\tilde{V}_R^2}{2\tilde{U}_{t\parallel}^2}\right),$$ (29)

where $\tilde{\Omega}_{wo} = \Omega_{wo}/\Omega_{e0}$, $\tilde{\omega}_{ph} = \omega_{ph}/\Omega_{e0}$, $\tilde{\omega}_0 = \omega_0/\Omega_{e0}$, $\tilde{U}_{t\parallel} = U_{t\parallel}/c$, and Ω_{e0} is the electron cyclotron frequency at the equator.

Finally, we can evaluate the nonlinear transition time using the wave amplitude obtained above. Using (7), we rewrite (25) as

$$T_N\Omega_{e0} = 2\pi\tau\left(\frac{\gamma\xi}{\chi\tilde{\omega}_0\tilde{V}_{\perp 0}\tilde{\Omega}_{w0}}\right)^{1/2}.$$ (30)

Thus, the formula for the optimum wave amplitude, which was originally derived for a rising chorus emission [*Omura and Nunn*, 2011], can be generalized for both rising and falling tone emissions.

2.2. Threshold Amplitude for Absolute Instability

The nonlinear triggering process described above takes place at a fixed position near the magnetic equator. The wave equation for the wave amplitude [*Omura et al.*, 2009, 2012] is

$$\frac{\partial\Omega_w}{\partial t} = \Gamma_N\Omega_w - V_g\frac{\partial\Omega_w}{\partial h},$$ (31)

where Γ_N is the nonlinear growth rate given by

$$\Gamma_N = \frac{|Q|\omega_{ph}^2}{2}\left(\frac{\xi}{\Omega_w\omega_0}\right)^{1/2}\frac{V_g}{U_{t\parallel}}\left(\tilde{V}_{\perp 0}\frac{\chi}{\pi\gamma}\right)^{3/2}\exp\left(-\frac{\gamma^2 V_R^2}{2U_{t\parallel}^2}\right).$$ (32)

The absolute instability, which grows in time at a fixed position, requires the right-hand side of (31) to be positive. Although (31) is valid for both rising ($Q > 0$) and falling ($Q < 0$) tones, the following analysis is only for rising tones. With an electron hill ($Q < 0$) in the phase space, the inhomogeneity due to the gradient of the magnetic field causes wave damping. Falling tones cannot be amplified in the downstream region from the equator. For the spatial gradient of the wave amplitude $\partial\Omega_w/\partial h$ in (31), we assume a condition that maximizes the convective nonlinear growth, namely, we neglect the first term on the right-hand side of (15), and setting $S = -0.4$, we assume

$$\Omega_w = \frac{cs_2}{0.4s_0\omega_0}\frac{\partial\Omega_e}{\partial h}.$$ (33)

Further assuming a parabolic variation of the dipole magnetic field around the equator as $\Omega_e = \Omega_{e0}(1 + ah^2)$, we obtain

$$\frac{\partial \Omega_w}{\partial h} = \frac{cs_2}{0.4s_0\omega_0} \frac{\partial^2 \Omega_e}{\partial h^2} = \frac{5cas_2\Omega_{e0}}{s_0\omega_0}, \tag{34}$$

where the coefficient $a = 4.5/(LR_E)^2$ is determined by the L shell and the Earth's radius R_E. Substituting (32) and (34) into (31), we obtain the threshold wave amplitude for the nonlinear wave growth which is given by

$$\tilde{\Omega}_{\text{th}} = \frac{100\pi^3\gamma^3\xi}{\chi^5\tilde{\omega}_0\tilde{\omega}_{\text{ph}}^4\tilde{V}_{\perp0}^5} \left(\frac{\tilde{a}s_2\tilde{U}_{t\parallel}}{Q}\right)^2 \exp\left(\frac{\gamma^2\tilde{V}_R^2}{\tilde{U}_{t\parallel}^2}\right), \tag{35}$$

where $\tilde{a} = ac^2/\Omega_{e0}^2$. We note that falling tones induced by an electron hill in the phase space cannot be amplified because of the negative value of S due to the gradient of the magnetic field in the downstream region from the equator. Therefore, the threshold (35) is only valid for rising tone emissions.

The seed waves of the hiss emissions are generated at the frequency for the maximum linear growth rate by an instability driven by the temperature anisotropy of hot electrons. In the linear growth process, the waves become coherent and then the wave amplitude exceeds the threshold for nonlinear wave growth, so that rising tones are generated initially. The rising tones grow to the optimum wave amplitude, expanding the bandwidth of the hiss emissions to higher frequencies until the threshold amplitude become close to the optimum value. The rising tones create electron holes, which result in a strong perturbation of the velocity distribution function. A local enhancement of the velocity distribution arises between the electron holes, which results in growth of falling tone emissions. Except for the lowest part of the frequency band, we may find both rising and falling tone emissions. As the mechanism for the initial frequency broadening, the rising tone emissions play an essential role. Therefore, the threshold works as a necessary condition for the generation of the hiss emissions.

A recent kinetic theory [*Yoon et al.*, 2014] shows that aperiodic electromagnetic fluctuations in an unmagnetized plasma are proportional to the electron density. In the plasmasphere, the electromagnetic thermal fluctuations at very low frequencies can be enhanced because of the much higher plasma density. Although the linear growth rate is very small because of the low density of the energetic electrons, the initial coherent wave can be generated near the frequency corresponding to the maximum linear growth rate from the enhanced thermal fluctuations. In Figure 2a, we plot the optimum wave amplitude and the threshold amplitude for different $\omega_{\text{pe}}/\Omega_{e0}$ values. Lines in red, green, and blue represent cases with $\omega_{\text{pe}}/\Omega_{e0} = 25, 15, 5$, respectively. For this calculation we assume the following parameters: $L = 4.3$, $Q = 0.1$, $U_{t\parallel} = 0.2c$, $V_{\perp0} = 0.5c$, and $N_h/N_c = 0.00004$, where N_c is the density of cold electrons. These parameters are the same as in Case 1 presented in section 4 except for the plasma frequency ω_{pe}. For each of the parameters, we find a frequency range satisfying $\Omega_{wo} > \Omega_{\text{th}}$, and the range shifts to lower frequencies as the plasma frequency increases. As shown in Figure 2a, the ratio of the plasma frequency to the cyclotron frequency $\omega_{\text{pe}}/\Omega_{e0}$ at the equator mostly controls the frequency profiles of the optimum wave amplitude. A larger ratio makes the frequency of the hiss emissions much lower. We note that the lowest frequency has the largest optimum amplitude.

The upper boundary of a hiss emission corresponds to the upper limit of the frequency range $\Omega_{wo} > \Omega_{\text{th}}$. The threshold amplitude for rising tone emissions determines the bandwidth of the hiss emission. This is because the frequency broadening starts from the low frequency of the maximum linear growth rate and extends to the upper limit via the triggering of the rising tone elements. As a result of the triggering of the falling tone elements from the initial frequency, the lower boundary of the hiss emission becomes lower than the initial frequency.

We plot the nonlinear transition time in Figure 2b so as to show the time scale of the nonlinear wave growth. The nonlinear transition time T_N becomes shorter for the higher $\omega_{\text{pe}}/\Omega_{e0}$. For $\omega_{\text{pe}}/\Omega_{e0} = 25$, we find $T_N = 200 \sim 400\Omega_{e0}^{-1}$, i.e., $3.5 \sim 7.0$ ms for the equatorial cyclotron frequency $f_{ce} = 9$ kHz, which is short enough to account for the time scale of the hiss elements $10 \sim 100$ ms [*Summers et al.*, 2014]. Since we find $\omega T_N < 2\pi$ at $\omega < 0.03\Omega_{e0}$ in Figure 2b, it is emphasized that formation of an electron hole/hill can take place even less than one wave period.

In Figure 2c we plot the linear growth rate for different plasma frequencies. We assume a bi-Maxwellian distribution function for the energetic electrons with a parallel thermal velocity $V_{t\parallel} = U_{t\parallel}/\gamma$ and a perpendicular
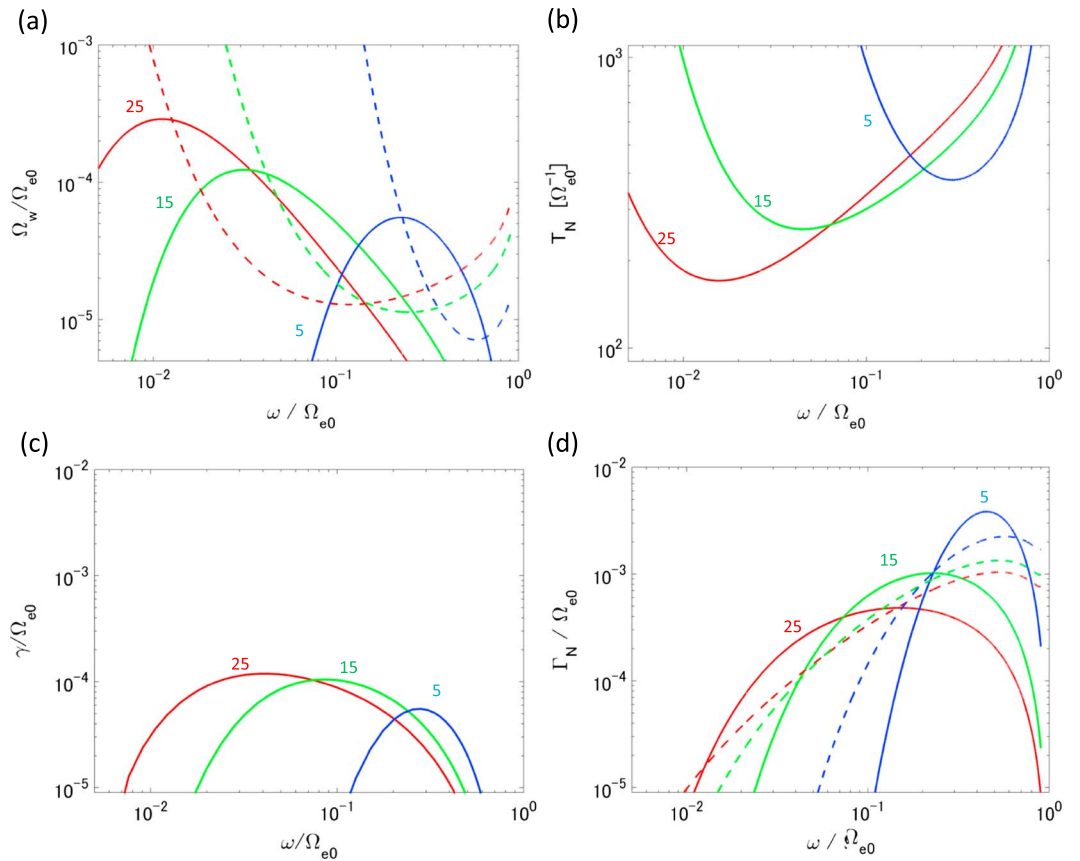
Figure 2. (a) Threshold wave amplitude (dashed line) and optimum wave amplitude (solid line), (b) nonlinear transition time, (c) linear growth rates, and (d) nonlinear growth rates at the threshold wave amplitude (solid line) and at the optimum wave amplitude (dashed line) for $\omega_{pe}/\Omega_{e0} = 5$ (blue), 15 (green), 25 (red) with parameters $\tau = 0.5$, $L = 4.3$ with $f_{ce} = 9$ kHz, $V_{\perp 0} = 0.5c$, $U_{t\parallel} = 0.2$, $N_h/N_c = 0.00004$, and $|Q| = 0.1$.

thermal velocity $V_{t\perp} = \sqrt{2/\pi}V_{\perp 0}$. The frequency corresponding to the maximum linear growth rate falls into the frequency range for nonlinear growth. The maximum linear growth takes place at a frequency higher than the lower limit of the frequency range for nonlinear wave growth. In Figure 2d, we plot the nonlinear growth rate Γ_N, defined by *Omura et al.* [2009], at the threshold amplitude and optimum wave amplitude, shown as solid and dashed lines, respectively. For a wide range of frequency, the nonlinear growth rate at the threshold amplitude is much greater than the linear growth rate.

We assumed a delta function in perpendicular velocity in the nonlinear theory, while we calculated the linear growth rate assuming a Maxwellian distribution function. The resonant electrons at low pitch angles cannot satisfy the condition for nonlinear wave trapping $|S| < 1$ because of small perpendicular velocities. Since only resonant electrons at high pitch angles are trapped by the wave potential and contribute to the nonlinear resonant current, the delta function at an average perpendicular velocity $V_{\perp 0}$ given by $\sqrt{\pi/2}V_{t\perp}$ is used for simplicity in the nonlinear theory.

2.3. Frequency Sweep Rate

In deriving the nonlinear growth rate near the equator, we have assumed a frequency variation satisfying (27). Without the frequency variation, electron holes or hills become symmetric in velocity phase space, and there arises no J_E for the wave growth. Substituting the optimum amplitude (29) into (27), we calculate absolute values of the frequency sweep rate for rising and falling tone elements generated as a result of the absolute instability near the equator. We use the same parameters as we have assumed in Figure 2. For comparison with observations, we convert the normalized values to real values assuming $f_{ce} = 9$ kHz, which is a typical value near the plasmapause. We show the frequency sweep rates for different values of ω_{pe} in Figure 3a. For the case $\omega_{pe}/\Omega_{e0} = 25$, the frequency sweep rate increases from 100 Hz/s to 800 Hz/s as the frequency increases over
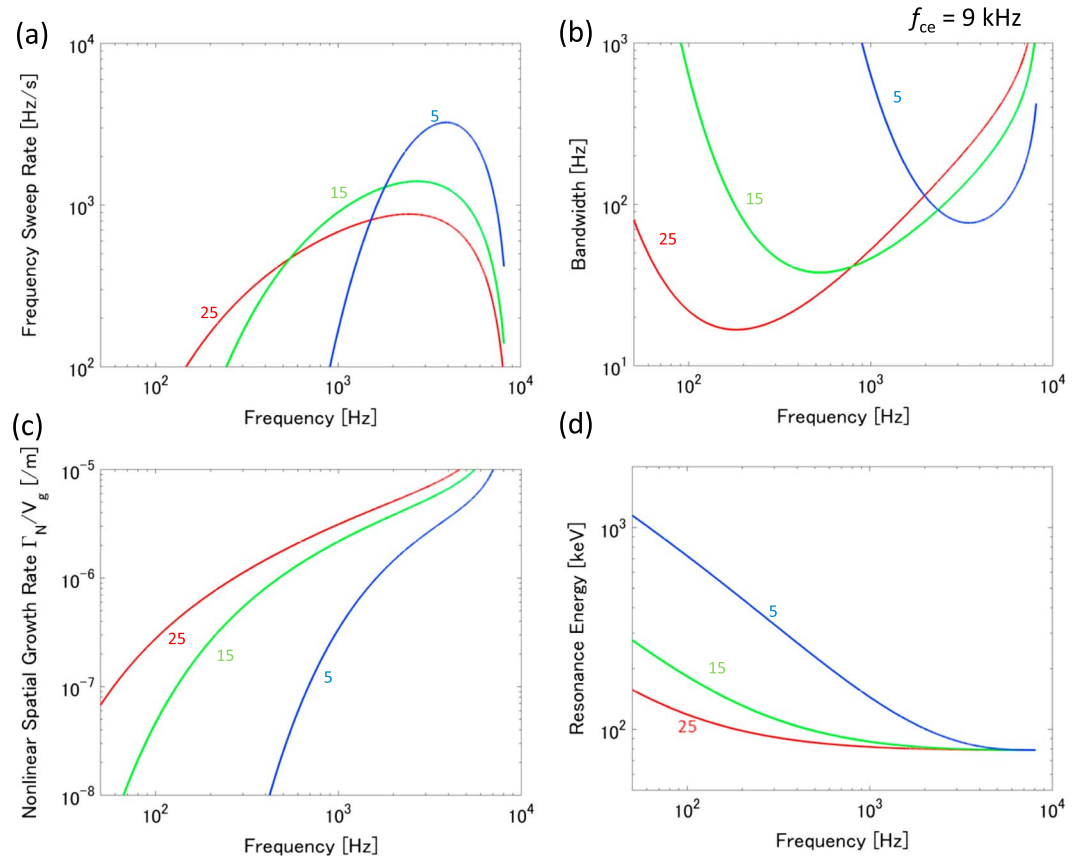
Figure 3. (a) Frequency sweep rate with the optimum wave amplitude, (b) frequency bandwidth corresponding to an electron hole in velocity phase space, (c) nonlinear spatial growth rate, and (d) energy of resonant electrons for $\omega_{pe}/\Omega_{e0} = 5$ (blue), 15 (green), and 25 (red) with the same parameters assumed in Figure 2.

the unstable range from 200 Hz to 1500 Hz. For the condition outside the plasmasphere, i.e., $\omega_{pe}/\Omega_{e0} = 5$, the frequency sweep rates take larger values corresponding to those of chorus emissions. In *Summers et al.* [2014] the sweep rates of rising and falling tone elements were calculated as $1-10$ kHz from the spectra of the fine structures. Some of the structures are conjunctions of two elements with slightly different frequencies. Such a conjunction appears as a single rising or falling tone element with a larger frequency variation and results in the overestimation of the sweep rates. We reexamined the phase variation of rising and falling tone elements applying narrower band-pass filter to extract independent hiss elements and found that the sweep rate is within a range of $200-800$ Hz/s in agreement with the theoretical estimation.

2.4. Separability Criterion

Using the optimum amplitude derived above, we can check if the separability criterion (2) for hiss is satisfied. We rewrite the criterion in terms of the wave frequencies and the frequency bandwidth $\Delta\omega$ corresponding to the size of the trapping potential in velocity phase space, i.e.,

$$|\omega^{j+1} - \omega^j| \gg \Delta\omega, \tag{36}$$

where

$$\Delta\omega = \left(\frac{\partial V_R}{\partial \omega_0}\right)^{-1}(2V_{tr}). \tag{37}$$

Using $V_{tr} = 2\omega_{tr}/k$ and $V_R = (\omega_0 - \Omega_e/\gamma)/k$, we have

$$\frac{\partial V_R}{\partial \omega_0} = \frac{1}{k} - \frac{1}{k^2}\left(\omega_0 - \frac{\Omega_e}{\gamma}\right)V_g^{-1}. \tag{38}$$

From (9), using the nonlinear trapping frequency $\omega_{tr} = \chi\sqrt{kV_\perp \Omega_{wo}/\gamma}$, we obtain

$$\Delta\omega = 4\omega_{tr}\left\{1 + \frac{\chi^2}{\omega_0}\left(\frac{\Omega_e}{\gamma} - \omega_0\right)\left[\xi^2 + \frac{\Omega_e}{2(\Omega_e - \omega_0)}\right]\right\}^{-1}. \tag{39}$$

We plot the frequency bandwidth in Figure 3b, where we assume the electron cyclotron frequency $f_{ce} = 9$ kHz and the same parameters used in Figure 2. For the case inside the plasmasphere with $\omega_{pe}/\Omega_{e0} = 25$, nonlinear wave growth takes place in the frequency range 100 Hz to 1.5 kHz, and the bandwidth varies $20 \sim 100$ Hz. Especially around 200 Hz, the bandwidth is less than 20 Hz, making it possible to generate multiple hiss elements with rising and falling tones in this frequency range. For the case outside the plasmasphere with $\omega_{pe}/\Omega_{e0} = 5$, on the other hand, wave growth is possible in the range of $2 \sim 6$ kHz, and the bandwidth is about 100 Hz. The narrow bandwidth of the nonlinear trapping potential is one of the necessary conditions for the generation of hiss emissions consisting of many coherent waves at different frequencies. Therefore, the high plasma density in the plasmasphere is more favorable for the generation of hiss emissions.

2.5. Nonlinear Wave Growth as Convective Instability

We also evaluate the nonlinear spatial growth rate Γ_N/V_g as plotted in Figure 3c, assuming the optimum amplitude shown in Figure 2a in calculating Γ_N. We can evaluate a minimum distance for a wave packet generated at the equator to grow through propagation. The minimum distance of several hundred kilometers is needed for the high-frequency part (> 1 kHz) to grow a few times larger. The lower frequency part of the wave spectrum cannot be amplified appreciably though propagation compared with the higher-frequency part.

Since the nonlinear growth rate under the assumption of rising tone emissions is significantly large, rising tone emissions should play a predominant role in forming a hiss band. The absolute instability of a rising tone emission can be connected smoothly to the convective instability, in which the wave grows in a frame of reference moving with the group velocity. However, a falling tone emission cannot maintain the nonlinear growth rate in propagating away from the equator because of the opposite signs of the frequency sweep rate and the spatial gradient of the magnetic field in the formula for the inhomogeneity factor S.

Whistler mode waves with constant frequencies grow from the thermal fluctuations with the linear growth rate shown in Figure 2c. The wave with the maximum linear growth rate becomes dominant and coherent. As soon as the amplitude becomes greater than the threshold amplitude, nonlinear wave growth takes place with an increasing frequency at a fixed position as an absolute instability. In the process of the frequency increase, the wave grows as long as the amplitude does not exceed the optimum wave amplitude appreciably. Waves generated by the absolute instability at the equator propagate away from the equator with the group velocity V_g, growing with the nonlinear growth rate Γ_N as indicated by the wave equation (31). The nonlinear growth rate at the optimum wave amplitude is small in the lower frequency range, while it becomes much larger than the linear growth rate in the higher frequency range as shown by the solid lines in Figure 2d. Convective nonlinear wave growth can take place effectively in the higher frequency range.

2.6. Kinetic Energy of Resonant Electrons

In the process of nonlinear wave growth, most of the resonant electrons lose energy, being scattered to lower pitch angles, while a fraction of phase-trapped electrons is accelerated to higher energy through nonlinear trapping [*Omura et al.*, 2007; *Summers and Omura*, 2007]. Those electrons scattered to lower pitch angles form an electron hole in the velocity phase space with their perpendicular velocities decreased substantially, falling into the loss cone as demonstrated by particle simulations [*Hikishima et al.*, 2009; *Hikishima and Omura*, 2012]. To evaluate the kinetic energy of resonant electrons with the average perpendicular velocity $V_{\perp 0}$, as represented by the velocity distribution function (10), we calculate the resonance energy E_R of whistler mode waves from the Lorentz factor of a resonant electron as

$$E_R = m_0 c^2\left[\left(1 - \tilde{V}_{\perp 0}^2 - \tilde{V}_R^2\right)^{-1/2} - 1\right], \tag{40}$$

where

$$\tilde{V}_R = \frac{\tilde{V}_p}{\tilde{V}_p^2 + \tilde{\omega}_0^2}\left\{\tilde{\omega}_0^2 - \sqrt{\tilde{\omega}_0^4 + \left(\tilde{V}_p^2 + \tilde{\omega}_0^2\right)\left(1 - \tilde{\omega}_0^2 - \tilde{V}_{\perp 0}^2\right)}\right\}. \tag{41}$$

We have plotted E_R as a function of frequency for $\omega_{pe}/\Omega_{e0} = 5, 15$, and 25 in Figure 3d. The lowest energy 79 keV is determined by $V_{\perp 0}/c = 0.5$. Because of the variation of the resonance velocity V_R over the broad
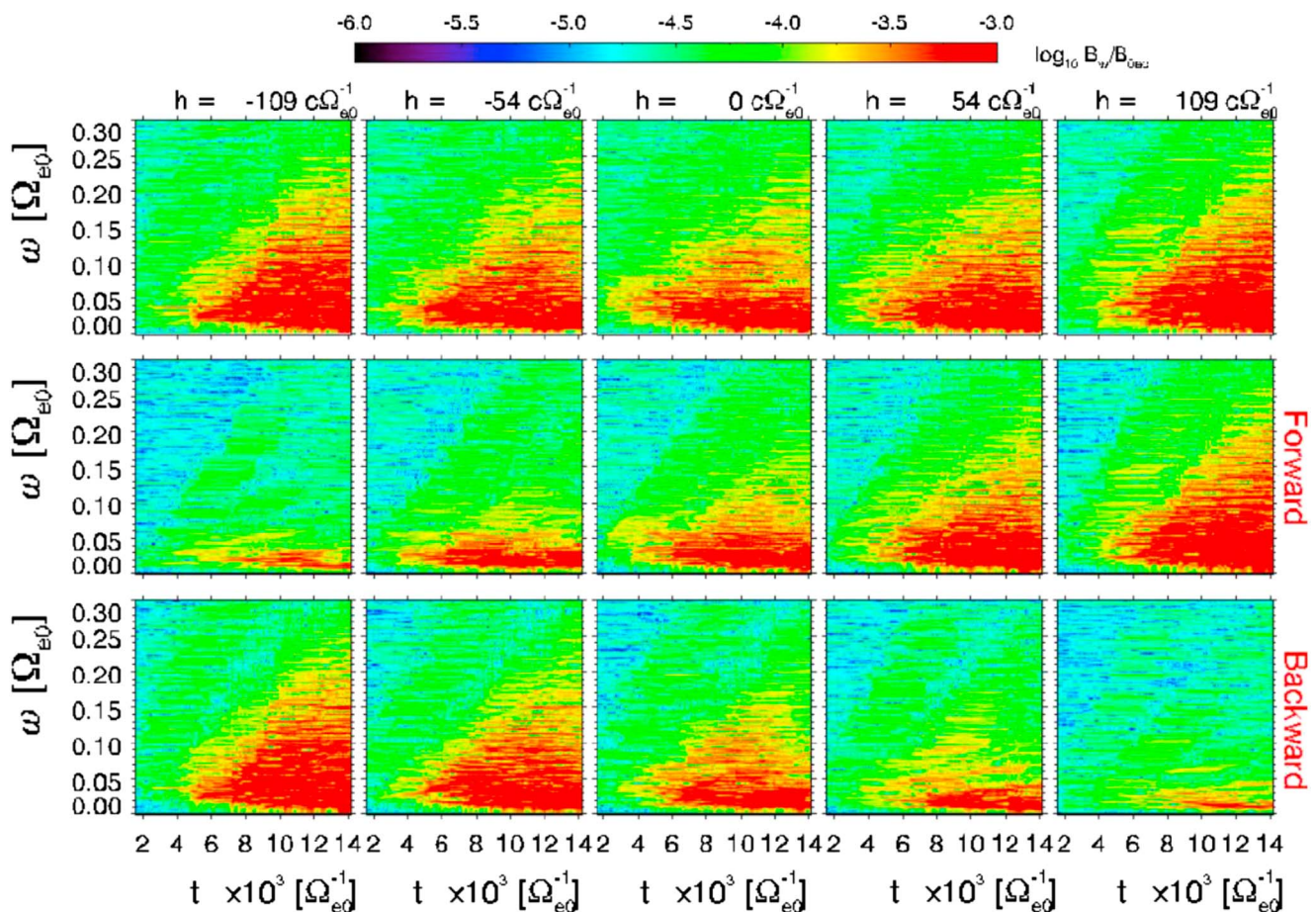
Figure 4. Electromagnetic particle simulation with anisotropic energetic electrons, a parabolic magnetic field, and the dense plasma condition $\omega_{pe}/\Omega_{e0} = 15$, showing (top row) the initial phase of hiss emissions with spectrum broadening due to nonlinear growth of many of short rising tone elements as well as falling tone elements. (top row) The emissions are started from spontaneously growing coherent waves due to the linear instability. Dynamic spectra of wave magnetic field are observed at different locations near the equator. The waves are separated into (middle row) forward and (bottom row) backward traveling components based on spatial helicities.

frequency range of hiss, the resonance energy likewise varies over a wide range. With a dense plasma condition $\omega_{pe}/\Omega_{e0} = 15 \sim 25$, the energy of resonant electrons generating hiss emissions above 100 Hz is about $100 \sim 200$ keV.

3. Particle Simulation of the Initial Phase of Hiss Emissions

An electromagnetic simulation used for chorus generation studies [*Hikishima et al.*, 2009, 2010; *Hikishima and Omura*, 2012] has been applied to a plasmaspheric condition $\omega_{pe}/\Omega_{e0} = 15$, and the initial result is presented in Figure 4. This figure shows the time evolution of the wave frequency spectra observed at different locations near the equator. The particle parameters of the simulation are $U_{t\parallel}/c = 0.51$, $V_{\perp 0}/c = 0.59$, and $n_h/n_c = 0.00074$. The gradient of the parabolic magnetic field is assumed to be $a = 1.1176 \times 10^{-7} (\Omega_{e0}/c)^2$. The simulation requires a large amount of computational resources. The simulation system consists of 32,768 grid points and 134,217,728 particles for each of the cold and hot electron species. The time step is $0.003/\Omega_{e0}$ and the number of time steps used is 5,242,880. Although we do not present detailed analyses of the simulation result in this paper, we have confirmed that the nonlinear growth process is taking place with a plasmaspheric condition. We find a broadening of the wave spectra starting with the frequency of the maximum linear growth rate. In the generation region near the equator, both forward and backward waves are excited. The wave spectra in Figure 4 (top row) are decomposed into forward and backward waves shown in Figures 4 (middle row) and 4 (bottom row), respectively. In the region slightly upstream from the equator ($h = 0$), falling tones are more prominent than rising tones in agreement with nonlinear growth theory based on the formation of electron hills for falling tones [*Nunn and Omura*, 2012]. In the downstream region, the wave

amplitudes of rising tones increase significantly as the waves propagate away from the equator. It is not clear that the emissions have evolved to be hiss emissions, because the simulation run has been started from an initial condition with an unstable particle distribution. We cannot therefore confirm a steady state where continuous hiss emissions are maintained by a continuous injection of fresh energetic electrons. Detailed analyses of the simulation results are currently being undertaken along with longer simulation runs, and the results will be reported in a separate paper.

4. Comparison With Plasmaspheric Hiss Observations

We have analyzed the wave form data obtained by the EMFISIS instrument [*Kletzing et al.*, 2013] on the Van Allen Probes. We use wave form data of 1 s to obtain characteristics of the hiss elements. We first transform three components of the magnetic field data to the parallel and perpendicular directions with respect to the local magnetic field. We separate the wave oscillations consisting of the two perpendicular components into narrow frequency ranges of 100 Hz bandwidth. Assuming that each frequency band only contains a single wave, we calculate the instantaneous wave frequency and amplitude for a segment containing a coherent wave oscillation.

Using a segment of a 1 s interval starting from 17:42:30 on 30 September 2012, we plot the instantaneous wave amplitude and frequency of hiss elements in Figure 5a. This hiss event is reported by *Ni et al.* [2014] and *Li et al.* [2013] as an unusual hiss event at the time of a magnetic storm. The three components of the magnetic field are transformed into one parallel and two perpendicular components with respect to the magnetic field, and each 100 Hz segment of the wave spectrum obtained by an FFT is transformed to a time series by an IFFT. The reconstructed time series of the two perpendicular components gives a time series of the wave vector in the plane perpendicular to the magnetic field. Using a time period between two adjacent zero crossings of one of the perpendicular components, we calculate the instantaneous frequency. If the frequency is within the range of the frequency band, we plot the magnitude of the perpendicular magnetic field by a dot at the instantaneous frequency. If the frequency is outside the frequency band, we discard it. Repeating the process for all zero crossings in 1 s and for all frequency bands, we obtained the scatter plot sown in Figure 5a. The distribution of the dots fluctuates with some peaks in the middle of each frequency band. This is because of overlaps of two or three hiss elements in each frequency band of 100 Hz. Therefore, the peaks do not represent real wave amplitudes of individual hiss elements. For comparison, we also plot in red the average amplitude calculated from the EMFISIS survey mode spectral density. This amplitude is calculated by multiplying each value by the spectral width at each frequency.

In Figure 5b we choose the L shell $L = 4.8$ and the plasma frequency 150 kHz, and the cyclotron frequency 6 kHz based on the observations. For the parameters describing the energetic electrons, we assume the density of energetic electrons $N_h/N_c = 0.0001$, the average perpendicular velocity $V_{\perp 0}/c = 0.5$, and we take a range of values of the parallel thermal momentum, namely, $U_{t\parallel}/c = 0.15, 0.20, 0.25$, and 0.30. We adjust these parameters to make the maximum wave amplitude and the frequency band close to the observed values. The parallel thermal momentum $U_{t\parallel}$ controls the gradient of the wave amplitude profile $\Omega_w(\omega)$. The average perpendicular velocity is determined so that the linear growth rate takes positive values. The density of energetic electrons determines the optimum wave amplitude as well as the threshold amplitude, thereby determining the upper limit of the hiss emission. The particle parameters that we assumed in fitting the optimum amplitude to the observed amplitude profile gives a kinetic energy about 100 keV, which agrees with the particle observation reported in Figure 1e of *Ni et al.* [2014].

We now study two cases of hiss emissions, as reported by *Summers et al.* [2014], on 18 and 21 February 2013. Case 1, with a duration of 1 s from 04:29:34 on 21 February, is an example of hiss observed very close to the magnetic equator. We plot the instantaneous wave amplitude as a function of frequency in Figure 6a. We can fit the optimum wave amplitude (blue line) and the threshold wave amplitude (black dashed line) to Case 1 as shown in Figure 6c, using parameters $L = 4.3$, $f_{ce} = 9$ kHz, $f_{pe} = 200$ kHz, $V_{\perp 0} = 0.5c$, $U_{t\parallel} = 0.2c$, and $N_h/N_c = 0.00004$. For Case 2, observed in an off-equatorial region with a duration of 1 s from 09:26:56, we find enhancement of the amplitude spectra for higher frequencies greater than 500 Hz as shown in Figure 6b. We first fit the optimum and threshold amplitudes to the observed frequency range of the hiss emission by using the parameter $L = 4.6$, $f_{ce} = 6$ kHz, $f_{pe} = 140$ kHz, $V_{\perp 0} = 0.5c$, $U_{t\parallel} = 0.15c$, and $N_h/N_c = 0.00007$ as shown in Figure 6d. We then take into account the effect of nonlinear convective wave growth from the
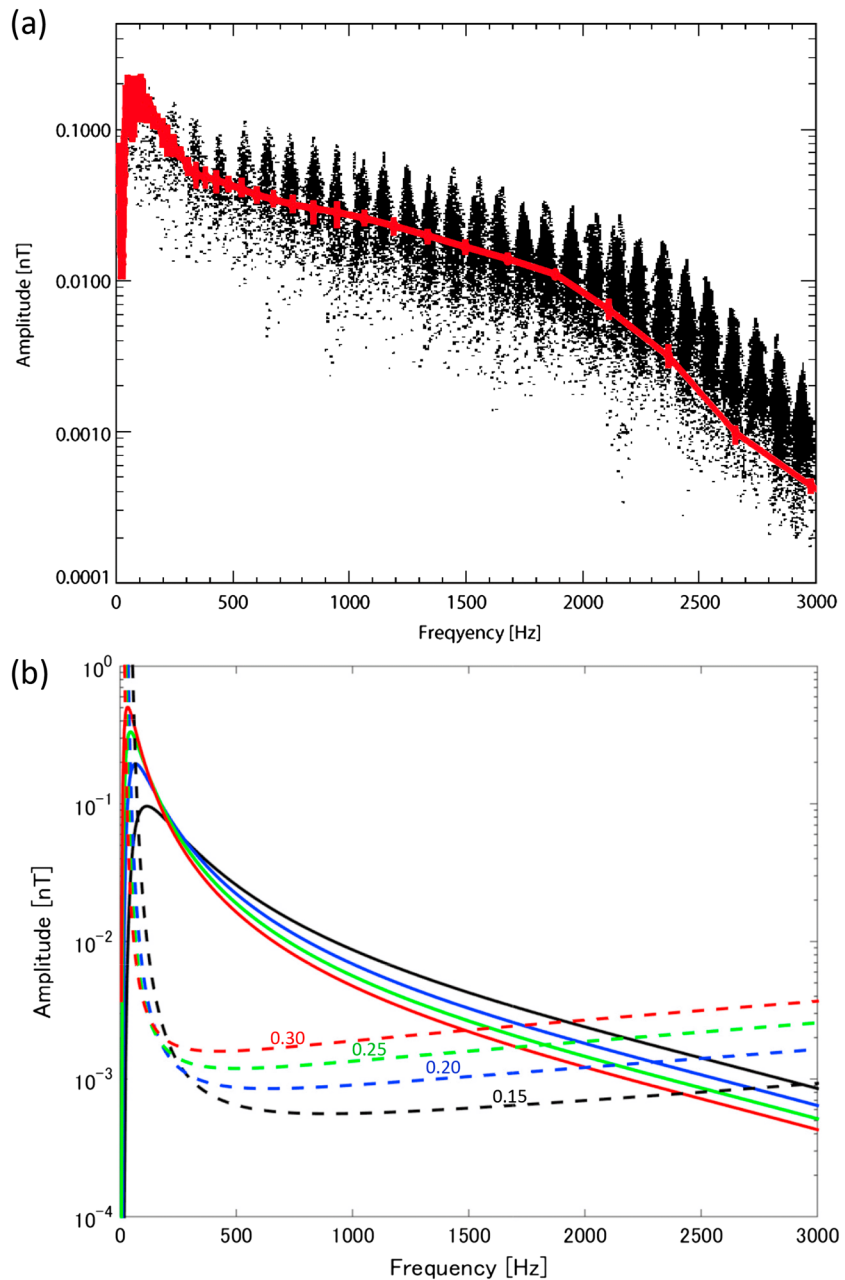
Figure 5. (a) Instantaneous wave amplitudes and frequencies of wave forms reconstructed from each of the 100 Hz segment of magnetic field spectrum density of hiss emissions observed by the Van Allen Probe A during a 1 s interval starting from 17:42:30 on 30 September 2012. The average amplitude calculated from the spectral density of three components of EMFISIS data in the survey mode is also plotted in red. (b) Optimum amplitudes with $\tau = 0.5$ and the threshold amplitude for triggering a rising tone element at $L = 4.8$ with $f_{ce} = 6$ kHz, $f_{pe} = 150$ kHz, $V_{\perp 0} = 0.5c$, $U_{t\parallel} = 0.15, 0.20, 0.25, 0.30c$, $N_h/N_c = 0.0001$, and $|Q| = 0.1$.

optimum amplitude attained at the equator. Using the nonlinear spatial growth rate shown in Figure 3d, we calculate the increased amplitude due to convection over a short distance of 300 km and plot this in red in Figure 6d. However, this is a rough evaluation obtained by using the largest possible nonlinear growth rate corresponding to $S = -0.4$ condition. This condition may not be satisfied in reality, and a more exact evaluation requires numerical integration of the wave equations involving the nonlinear resonant current [*Summers et al.*, 2012]. In both cases, we have assumed $\tau = 0.5$, $|Q| = 0.1$, and $V_{\perp 0}/c = 0.5$, which gives a resonance energy about 100 keV.
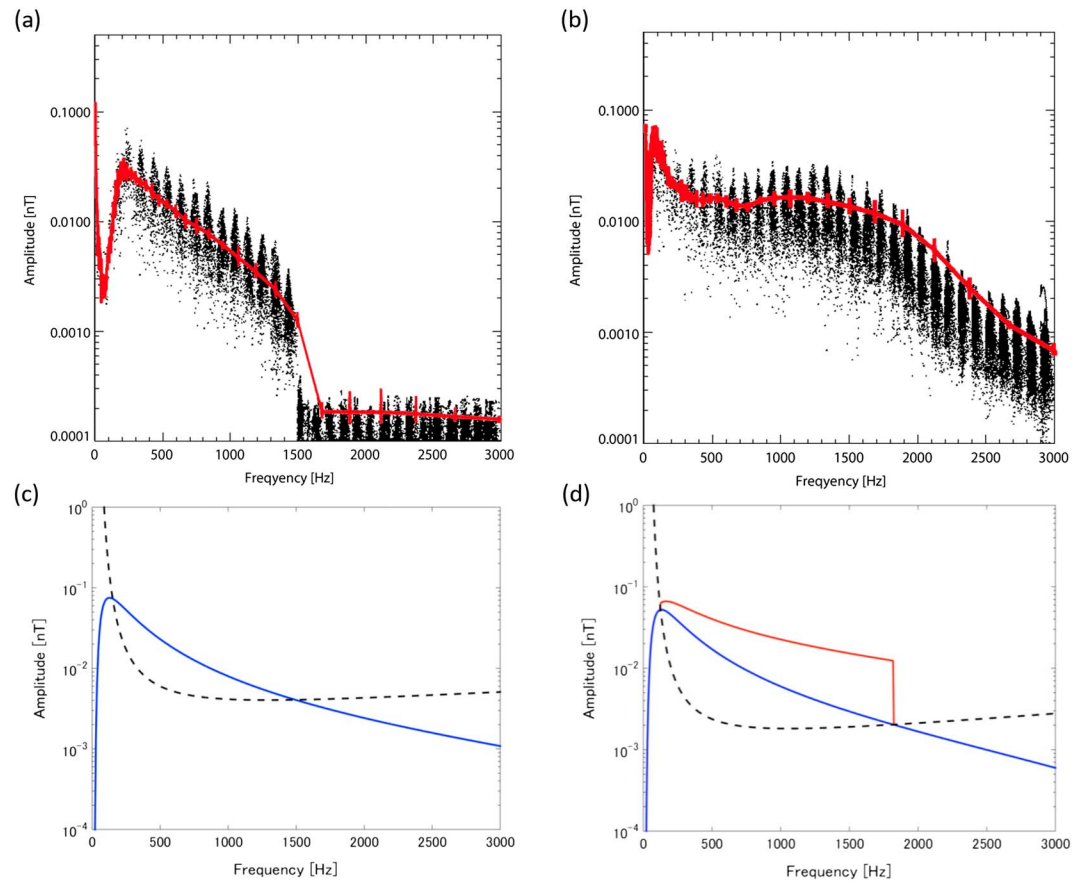
Figure 6. Instantaneous wave amplitudes (black) and averaged amplitudes (red) as functions of frequencies, which are obtained by the same method used in Figure 5, for hiss emissions (a) Case 1 and (b) Case 2 in *Summers et al.* [2014]. (c, d) Optimum amplitudes (solid blue line) and threshold amplitudes (dashed black line) corresponding to Case 1 and Case 2, respectively. In Case 2, the amplitude profile after nonlinear convective growth over a distance of 300 km is also plotted in red. The assumed parameters are Case 1: $L = 4.3$, $f_{ce} = 9$ kHz, $f_{pe} = 200$ kHz, $V_{\perp 0} = 0.5c$, $U_{t\parallel} = 0.2c$, $N_h/N_c = 0.00004$ and Case 2: $L = 4.6$, $f_{ce} = 6$ kHz, $f_{pe} = 140$ kHz, $V_{\perp 0} = 0.5c$, $U_{t\parallel} = 0.15c$, $N_h/N_c = 0.00007$. In both cases, $\tau = 0.5$, and $|Q| = 0.1$.

5. Summary and Discussion

We have obtained an optimum wave amplitude that can trigger rising and falling tone hiss elements. The temperature anisotropy of energetic electrons near the equator induces the linear whistler mode instability resulting in a coherent wave growing from thermal fluctuations. When the wave amplitude exceeds the threshold wave amplitude given by (35), an electromagnetic electron hole is formed in velocity phase space, resulting in gradual formation of the negative J_B and corresponding positive frequency shift. The positive frequency sweep rate makes the electron hole asymmetric with $S \sim -0.4$, inducing the negative J_E, which causes wave growth as an absolute nonlinear instability near the equator. As soon as the wave amplitude reaches the optimum wave amplitude the absolute instability saturates, but the generated wave packet can grow due to the nonlinear growth rate through propagation. The generation of rising tone emissions at the equator is repeated at progressively higher frequencies making the frequency range of hiss emissions gradually wider. The process of spectral broadening has been confirmed to take place by the particle simulation in section 3. The upper limit of hiss emissions is determined by the frequency range in which the optimum amplitude is greater than the threshold amplitude. This broadening over the finite band yields the spectral characteristics of observed hiss emissions.

The nonlinear wave growth process requires a coherent wave with a finite amplitude greater than the threshold amplitude, which triggers the wave growth through formation of an electron hole for a rising tone emission or an electron hill for a falling tone emission. The triggering wave can be a wave spontaneously growing from the thermal fluctuations or an external wave propagating into the plasmasphere such as a

chorus wave from the outside of the plasmasphere or whistlers from the atmospheric lightning. Since the linear growth rate is very small in the present study, the wave growth process from the thermal fluctuations proceeds very slowly, while the nonlinear growth rate is much higher than the linear growth rate as shown in Figures 2c and 2d.

As we found in Figure 2d, the nonlinear growth rate maximizes at a frequency higher than the frequency of the maximum linear growth rate. At higher frequencies, many rising tone elements are triggered, and they grow up to the optimum wave amplitude. The spectrum shape changes with increasing frequencies. Near the equator, the spectrum shape as a function of the frequency is determined by the frequency profile of the optimum wave amplitude. The tendency of decreasing amplitude with increasing frequency is found in hiss emissions reported in the published literature [*Thorne et al.*, 1973; *Ni et al.*, 2014; *Li et al.*, 2014; *Tsurutani et al.*, 2015]. Through the wave spectrum, shape changes from the profile of the optimum wave amplitude through propagation from the equator to higher latitudes because of the convective growth at higher frequencies.

In developing the nonlinear wave growth theory, we have assumed many coherent waves in a purely field-aligned direction near the magnetic equator, where the waves at the same locations have different frequencies satisfying the separability criterion. The phase organization of the particles takes place in the transverse plane perpendicular to the magnetic field. As the waves propagate away from the equator, the wave normal angles deviate from the parallel direction, and there arise longitudinal interactions involving parallel electric fields. In the presence of energetic electrons with a Maxwellian distribution function, the waves can be expected to undergo Landau damping at the phase velocity $\omega/k_{\parallel}$ as a result of the parallel electric fields. After the absolute instability and the convective growth takes place near the equator, the wave amplitudes should gradually decrease through Landau damping. However, the damping is only limited to lower latitudes, because the parallel velocities of energetic electrons decrease due to adiabatic motion. A smaller number of electrons then interact with the wave at the phase velocity.

A simulation study by *Katoh and Omura* [2013] shows generation of broadband waves outside the plasmasphere ($\omega_{pe}/\Omega_{e0} = 4$). The simulation demonstrates the broadening of the frequency spectra due to the many triggering of rising tone chorus emissions.

Gao et al. [2014] reported supporting evidence for the nonlinear wave growth mechanism generating hiss-like emissions. The higher density of energetic electrons results in a wider gap between the optimum wave amplitude and the threshold wave amplitude, and this is a favorable condition for triggering many rising tones which are observed as hiss-like emissions. Essentially, the same mechanism takes place in the generation process of plasmaspheric hiss emissions.

References

Bortnik, J., R. M. Thorne, and N. P. Meredith (2008), The unexpected origin of plasmaspheric hiss from discrete chorus emissions, *Nature*, *452*, 62–66, doi:10.1038/nature06741.

Bortnik, J., W. Li, R. M. Thorne, V. Angelopoulos, C. Cully, J. Bonnell, O. Le Contel, and A. Roux (2009), An observation linking the origin of plasmaspheric hiss to discrete chorus emissions, *Science*, *324*, 775–778, doi:10.1126/science.1171273.

Chen, L., et al. (2014), Generation of unusually low frequency plasmaspheric hiss, *Geophys. Res. Lett.*, *41*, 5702–5709, doi:10.1002/2014GL060628.

Gao, X., W. Li, R. M. Thorne, J. Bortnik, V. Angelopoulos, Q. Lu, X. Tao, and S. Wang (2014), Statistical results describing the bandwidth and coherence coefficient of whistler mode waves using THEMIS waveform data, *J. Geophys. Res. Space Physics*, *119*, 8992–9003, doi:10.1002/2014JA020158.

Church, S. R., and R. M. Thorne, (1983), On the origin of plasmaspheric hiss: Ray path integrated amplification, *J. Geophys. Res.*, *88*(A10), 7941-7957, doi:10.1029/JA088iA10p07941.

Draganov, A. B., U. S. Inan, V. S. Sonwalkar, and T. F. Bell (1992), Magnetospherically reflected whistlers as a source of plasmaspheric hiss, *Geophys. Res. Lett.*, *19*, 233-236, doi:10.1029/91GL03167.

Hikishima, M., Y. Omura, and D. Summers (2010), Self-consistent particle simulation of whistler mode triggered emissions, *J. Geophys. Res.*, *115*, A12246, doi:10.1029/2010JA015860.

Hikishima, M., S. Yagitani, Y. Omura, and I. Nagano (2009), Full particle simulation of whistler-mode rising chorus emissions in the magnetosphere, *J. Geophys. Res.*, *114*, A01203, doi:10.1029/2008JA013625.

Hikishima, M., and Y. Omura (2012), Particle simulations of whistler-mode rising-tone emissions triggered by waves with different amplitudes, *J. Geophys. Res.*, *117*, A04226, doi:10.1029/2011JA017428.

Huang, C. Y., C. K. Goertz, and R. R. Anderson (1983), A theoretical study of plasmaspheric hiss generation, *J. Geophys. Res.*, *88*, 7927–7940, doi:10.1029/JA088iA10p07927.

Katoh, Y., and Y. Omura (2013), Effect of the background magnetic field inhomogeneity on generation processes of whistler-mode chorus and broadband hiss-like emissions, *J. Geophys. Res. Space Physics*, *118*, 4189–4198, doi:10.1002/jgra.50395.

Kennel, C. F., and H. E. Petschek (1966), Limit on stably trapped particle fluxes, *J. Geophys. Res.*, *71*(1), 1–28, doi:10.1029/JZ071i001p00001.

Kletzing, C. A., et al. (2013), The Electric and Magnetic Field Instrument Suite and Integrated Science (EMFISIS) on RBSP, *Space Sci. Rev.*, *179*, 127–181, doi:10.1007/s11214-013-9993-6.

Laakso, H., O. Santolik, R. Horne, I. Kolmasová, P. Escoubet, A. Masson, and M. Taylor (2015), Identifying the source region of plasmaspheric hiss, *Geophys. Res. Lett.*, *42*, 3141–3149, doi:10.1002/2015GL063755.

Li, W., et al. (2013), An unusual enhancement of low-frequency plasmaspheric hiss in the outer plasmasphere associated with substorm-injected electrons, *Geophys. Res. Lett.*, *40*, 3798–3803, doi:10.1002/grl.50787.

Li, W., et al. (2014), Quantifying hiss-driven energetic electron precipitation: A detailed conjunction event analysis, *Geophys. Res. Lett.*, *41*, 1085–1092, doi:10.1002/2013GL059132.

Ni, B., et al. (2014), Resonant scattering of energetic electrons by unusual low-frequency hiss, *Geophys. Res. Lett.*, *41*, 1854–1861, doi:10.1002/2014GL059389.

Nunn, D., and Y. Omura (2012), A computational and theoretical analysis of falling frequency VLF emissions, *J. Geophys. Res.*, *117*, A08228, doi:10.1029/2012JA017557.

Omura, Y., D. Nunn, H. Matsumoto, and M. J. Rycroft (1991), A review of observational, theoretical and numerical studies of VLF triggered emissions, *J. Atmos. Terr. Phys.*, *53*, 351–368.

Omura, Y., Y. Katoh, and D. Summers (2008), Theory and simulation of the generation of whistler-mode chorus, *J. Geophys. Res.*, *113*, A04223, doi:10.1029/2007JA012622.

Omura, Y., M. Hikishima, Y. Katoh, D. Summers, and S. Yagitani (2009), Nonlinear mechanisms of lower-band and upper-band VLF chorus emissions in the magnetosphere, *J. Geophys. Res.*, *114*, A07217, doi:10.1029/2009JA014206.

Omura, Y., and D. Nunn (2011), Triggering process of whistler mode chorus emissions in the magnetosphere, *J. Geophys. Res.*, *116*, A05205, doi:10.1029/2010JA016280.

Omura, Y., N. Furuya, and D. Summers (2007), Relativistic turning acceleration of resonant electrons by coherent whistler mode waves in a dipole magnetic field, *J. Geophys. Res.*, *112*, A06236, doi:10.1029/2006JA012243.

Omura, Y., D. Nunn, and D. Summers (2012), Generation processes of whistler-mode chorus emissions: Current status of nonlinear wave growth theory, in *Dynamics of the Earth's Radiation Belts and Inner Magnetosphere*, edited by D. Summers et al., *Geophys. Monogr. Ser.*, vol. 199, AGU, Washington, D. C., doi:10.1029/2012GM001347.

Santolik, O., M. Parrot, L. R. O. Storey, J. S. Pickett, and D. A. Gurnett (2001), Propagation analysis of plasmaspheric hiss using Polar PWI measurements, *Geophys. Res. Lett.*, *28*, 1127–1130.

Santolik, O., J. Chum, M. Parrot, D. A. Gurnett, J. S. Pickett, and N. Cornilleau-Wehrlin (2006), Propagation of whistler mode chorus to low altitudes: Spacecraft observations of structured ELF hiss, *J. Geophys. Res.*, *111*, A10208, doi:10.1029/2005JA011462.

Summers, D., and Y. Omura (2007), Ultra-relativistic acceleration of electrons in planetary magnetospheres, *Geophys. Res. Lett.*, *34*, L24205, doi:10.1029/2007GL032226.

Summers, D., Y. Omura, Y. Miyashita, and D.-H. Lee (2012), Nonlinear spatio-temporal evolution of whistler mode chorus waves in Earth's inner magnetosphere, *J. Geophys. Res.*, *117*, A09206, doi:10.1029/2012JA017842.

Summers, D., Y. Omura, S. Nakamura, and C. A. Kletzing (2014), Fine structure of plasmaspheric hiss, *J. Geophys. Res. Space Physics*, *119*, 9134–9149, doi:10.1002/2014JA020437.

Thorne, R. M., E. J. Smith, R. K. Burton, and R. E. Holzer (1973), Plasmaspheric hiss, *J. Geophys. Res.*, *78*(10), 1581–1596.

Tsurutani, B. T., B. J. Falkowski, J. S. Pickett, O. Santolik, and G. S. Lakhina (2015), Plasmaspheric hiss properties: Observations from Polar, *J. Geophys. Res. Space Physics*, *120*, 414–431, doi:10.1002/2014JA020518.

Yoon, P. H., R. Schlickeiser, and U. Kolberg (2014), Thermal fluctuation levels of magnetic and electric fields in unmagnetized plasma: The rigorous relativistic kinetic theory, *Phys. Plasmas*, *21*, 032109, doi:10.1063/1.4868232.